Manifestation of the Aharonov-Bohm effect in the interaction of moving charges with a semiconductor nanotube with dielectric filling

Yu. O. Averkov,[1,2,*] Yu. V. Prokopenko,[1] V. M. Yakovenko,[1] and V. A. Yampol'skii[1,2]

[1]*O. Ya. Usikov Institute for Radiophysics and Electronics, National Academy of Sciences of Ukraine, 61085 Kharkiv, Ukraine*

[2]*V. N. Karazin Kharkiv National University, 61077 Kharkiv, Ukraine*

(Received 20 March 2023; revised 17 July 2023; accepted 7 August 2023; published 17 August 2023)

We theoretically study the Aharonov-Bohm effect manifestation in the interaction of a moving nonrelativistic electron and a tubular electron beam with electromagnetic eigenmodes in a semiconductor nanotube with dielectric filling placed in a coaxial dc magnetic field. The calculations are performed taking into account the effect of delay of electromagnetic waves and collisions of electrons in a nanotube. First, we have shown that collisions of electrons lead to a significant transformation of the eigenmode spectrum of the structure under study in comparison with the collisionless case. In particular, dissipative (leaky) modes with phase velocities greater than the speed of light in vacuum appear in the spectrum. It has been established that the number of branches with negative (anomalous) dispersion in the eigenmode spectrum oscillates when changing the number of magnetic flux quanta in a nanotube with a period equal to one magnetic flux quantum. Second, an analysis of the expressions for the power of energy loss of a single moving electron and the rate of increase in the kinetic instability of an electron tubular beam due to their interaction with the studied eigenmodes showed that these quantities also oscillate when changing the number of magnetic flux quanta. These oscillations are the result of the Aharonov-Bohm effect.

DOI: 10.1103/PhysRevB.108.075420

I. INTRODUCTION

A paper by Aharonov and Bohm [1], published more than 50 years ago, took a fresh look at the role of electromagnetic field potentials in quantum phenomena. They first pointed out that the electrons could be affected by electromagnetic potentials without their coming into contact with actual force fields. This prediction was confirmed in subsequent interference experiments of coherent electronic beams wrapping miniature solenoids as well as in later, similar experiments using a tiny toroidal magnet [2–4]. It is worthwhile to note that, in the original 1959 paper, the magnetic as well as electric versions of the effect were considered, and, as was demonstrated later, both versions of the Aharonov-Bohm effect had so-called duals such as the Aharonov-Casher effect and the neutron-scalar effect (see review [5] and references therein).

Note that conducting nanotubes and quantum rings occupy a special place in the physics of low-dimensional systems due to the non-simply-connected area of electron movement. This leads, in the presence of the magnetic field, to phenomena that are consequences of the Aharonov-Bohm effect. Therefore, since the first solid-state manifestation of the Aharonov-Bohm effect for electron circulation in a mesoscopic nonsuperconducting metal rings [6], this effect has been actively investigated in a variety of mesoscopic systems. For instance, in recent decades, the Aharonov-Bohm oscillations of conductance matrix elements in ballistic graphene and phosphorene quantum rings, as well as in topological quantum rings in silicene and bilayer graphene, were studied in Refs. [7–9]. The possibility of the Aharonov-Bohm effect for excitons in a semiconductor quantum ring dressed by circularly polarized light was theoretically demonstrated in Ref. [10]. The influence of the Aharonov-Bohm effect on magnetoconductance, the quantum Hall effect, and Coulomb blockade in topological insulator nanocones were studied in Ref. [11]. The Aharonov-Bohm effects in three-dimensional higher-order topological insulators and in mesoscopic Bose-Einstein condensates were investigated in Refs. [12,13]. Topology and its detection in a dissipative Aharonov-Bohm chain was considered in Ref. [14].

The study of the Aharonov-Bohm effect in structures containing carbon nanotubes is of particular interest. This is due to a number of unique properties of such structures, making them promising candidates for creating a new element base for modern micro- and nanoelectronics (see, e.g., Refs. [15,16]). The measurement of magnetoresistance oscillations in individual multiwalled nanotubes caused by the Aharonov-Bohm effect was first made in Ref. [17]. The Fano resonance in crossed carbon nanotubes was studied in Ref. [18]. It was shown that the conductance peak is sensitive to the external magnetic field and exhibits Aharonov-Bohm-type oscillations. The Aharonov-Bohm splitting of the exciton peak in metallic carbon nanotubes was studied in Ref. [19]. The Aharonov-Bohm interferometer based on waveguides created by gating graphene with carbon nanotubes was proposed in Ref. [20].

Given the technological importance of semiconductors for the realization of nanoelectronics devices, semiconductor nanotubes alongside carbone nanotubes have been the subject of intense experimental and theoretical research (see, e.g., Refs. [21–23]). Note that semiconductor nanotubes and other

*Corresponding author: yuriyaverkov@gmail.com

two-dimensional semiconductor structures can be produced from silicon atoms forming unit cells similar to honeycombs, i.e., the same cells as in structures based on graphene [24–27]. Silicon nanotubes can be used in nanomedicine, e.g., for bioseparation, drug delivery, imaging, and other biomedical applications [21]. In addition, silicon nanotubes are promising as anode material in batteries [22] and silicon nanotubes, which are doped by transition-metal atoms, demonstrate magnetism and become attractive for use as nanoscale magnets [23].

In Ref. [28], the role of the Aharonov-Bohm effect in the dispersion properties of surface plasmons in semiconductor and carbon nanotubes was first studied theoretically in electrostatic approximation. It was demonstrated that the surface plasmon frequency as well as the Fermi energy of the degenerate electron gas oscillate with a change of the magnetic flux in the nanotube. Note that under Fermi energy oscillations, the equilibrium surface electron density was supposed to be given. As was stressed in this paper, the spatial dispersion of nanotube conductivity tensor components plays a key role in such oscillations.

In our previous papers [29,30], we have theoretically studied the manifestation of the Aharonov-Bohm effect in the eigenmode spectrum of a semiconductor nanotube with dielectric filling placed in a coaxial dc magnetic field. The main differences between our approach in the analysis of the eigenmode spectrum and the approach used in Ref. [28] were as follows. First, we supposed that the inner cavity of the nanotube was filled with a solid-state dielectric. Second, we have taken into account the retardation effects of the electromagnetic fields under the derivation of the dispersion equation, which described both the bulk-surface and the surface electromagnetic eigenmodes. We have shown that, in particular, the Aharonov-Bohm effect manifested itself in the oscillations of the number of dispersion branches with the change of the magnetic flux value in the nanotube. Hereafter, we describe the results of Refs. [29,30] in more detail.

In the present work, we consider the manifestation of the Aharonov-Bohm effect under the interaction of charged particles with a semiconductor nanotube filled with a solid-state dielectric. Unlike Refs. [29,30], now we take into account the electron collisions in the nanotube in order to correctly calculate the energy loss of an electron under the excitation of the electromagnetic waves in the structure. We show that the electron energy loss, as well as the increment of the kinetic instability in the case of propagation of a tubular electron beam along the structure, oscillate with a change in the number of magnetic flux quanta in the nanotube. In addition, we demonstrate that taking into account the electron collisions in the nanotube gives rise to the emergence of a new branch of the bulk-surface waves closely resembling the well-known Zenneck's wave [31].

II. STATEMENT OF THE PROBLEM: SPECTRUM OF THE EIGENWAVES

Consider a nonmagnetic dielectric cylinder of radius ρ_c occupying the space region $0 \leqslant \rho \leqslant \rho_c$, $0 \leqslant \varphi \leqslant 2\pi$, and $|z| < \infty$ (the z axis is directed along the cylinder axis). We suppose that the cylinder is made of a solid-state isotropic

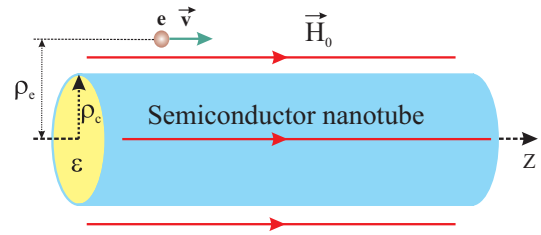

FIG. 1. Geometry of the problem.

nonmagnetic material with real permittivity ε and there is an infinitely thin semiconductor layer on the lateral surface of the cylinder. This waveguide is located in the vacuum in an external dc magnetic field $\vec{H}_0$ directed parallel to its axis (see Fig. 1).

A point charge moves in the vacuum parallel to the cylinder symmetry axis at a distance ρ_e from the axis with velocity $v \ll c$ (here c is the velocity of light in the vacuum). The electron charge density in the vacuum region is determined by the formula

$$Q_e(\vec{r},t) = en_e(\vec{r},t) = e\delta(\vec{\rho}-\vec{\rho}_e)\delta(z-vt), \tag{1}$$

where e is the electron charge and $\delta(x)$ is the Dirac delta function.

We describe the interaction between the moving electron and the structure eigenmodes using the Maxwell equations,

$$\mathrm{rot}\vec{H}(\vec{r},t) = \frac{1}{c}\frac{\partial}{\partial t}\vec{D}(\vec{r},t) + \frac{4\pi}{c}\vec{j}(\vec{r},t), \tag{2}$$

$$\mathrm{rot}\vec{E}(\vec{r},t) = -\frac{1}{c}\frac{\partial}{\partial t}\vec{H}(\vec{r},t), \tag{3}$$

$$\mathrm{div}\,\vec{D}(\vec{r},t) = 4\pi eN(\vec{r},t), \tag{4}$$

$$\mathrm{div}\,\vec{H}(\vec{r},t) = 0, \tag{5}$$

concurrent with the linearized continuity equation

$$e\frac{\partial N(\vec{r},t)}{\partial t} + \mathrm{div}\vec{j}(\vec{r},t) = 0, \tag{6}$$

where $\vec{E}(\vec{r},t)$ and $\vec{H}(\vec{r},t)$ are the electric and magnetic field vectors, and $\vec{D}(\vec{r},t)$ is the electric displacement vector. The current density exists in the vacuum region, at $(\rho > \rho_c)$, due to the moving point charge,

$$\vec{j}(\vec{r},t) = (0,0,Q_e(\vec{r},t)v), \tag{7}$$

and within the semiconductor nanotube in the form of surface current,

$$\vec{j}(\vec{r},t) = (0,\vec{j}_\tau(\vec{r},t)), \quad \vec{j}_\tau(\vec{r},t) = \vec{j}_\tau^{2D}(\varphi,z,t)\delta(\rho-\rho_c). \tag{8}$$

The electron density $N(\vec{r},t)$ is $n_e(\vec{r},t)$ in the vacuum region, at $(\rho > \rho_c)$, and $N(\vec{r},t) = n^{2D}(\varphi,z,t)\delta(\rho-\rho_c)$ in the semiconductor nanotube, at $(\rho < \rho_c)$, where $n^{2D}(\varphi,z,t)$ is the 2D density of charge carriers.

The displacement vector $\vec{D}(\vec{r},t)$ is connected to the electric field $\vec{E}(\vec{r},t)$ by the local relation,

$$\vec{D}(\vec{r},t) = \varepsilon\vec{E}(\vec{r},t). \tag{9}$$

The question about the conductivity of the surface conducting layer in a dc magnetic field is considered below.

A. Main equations for eigenmodes

We first study the spectra of electromagnetic eigenwaves in a semiconductor nanotube with dielectric filling. To find the dispersion equation for eigenmodes, it is necessary to use the boundary conditions for electric and magnetic fields at $\rho = \rho_c$. We use four boundary conditions describing the continuity of the tangential components of the electric field, $E_\varphi(\vec{r}, t)$, $E_z(\vec{r}, t)$, and the jumps of the ρ-component $D_\rho(\vec{r}, t)$ of the electric displacement vector and of the z-component $H_z(\vec{r}, t)$ of the magnetic field, caused by the presence of charges and currents on the surface of the semiconductor nanotube (see Ref. [30]).

We represent all field components as the superpositions of space-time harmonics, e.g.,

$$\vec{E}(\vec{r}, t) = \sum_{n=-\infty}^{\infty} \int_{-\infty}^{\infty} \int_{-\infty}^{\infty} \vec{E}_n(\rho, q_z, \omega) \times \exp[i(q_z z + n\varphi - \omega t)] dq_z d\omega, \quad (10)$$

where ω, q_z, and n are the frequency, longitudinal wave number, and spatial harmonic number (coinciding with the azimuthal mode index), respectively.

Taking into account expansion (10), we can rewrite Eqs. (2)–(5) for the axial spectral components of the fields in the regions $\rho < \rho_c$ and $\rho > \rho_c$ in the form

$$\hat{\Delta} E_{zn}(\rho, q_z, \omega) = 0, \quad \hat{\Delta} H_{zn}(\rho, q_z, \omega) = 0, \quad (11)$$

where

$$\hat{\Delta} = \frac{1}{\rho} \frac{\partial}{\partial \rho} \rho \frac{\partial}{\partial \rho} + \left(q_\nu^2 - \frac{n^2}{\rho^2} \right),$$

$\nu = 1, 2$; $q_\nu^2 = \varepsilon_\nu \omega^2 / c^2 - q_z^2$ is the squared transverse wave number, $\varepsilon_1 = \varepsilon$ (cylinder filling), and $\varepsilon_2 = 1$ (vacuum). For $q_\nu^2 > 0$, expressions (11) have the form of the Bessel equations, and for $q_\nu^2 < 0$ they are the modified Bessel equations. In our case, $q_2^2 < 0$ because we consider the case when the condition $\omega^2 < c^2 q_z^2$ is satisfied. The eigenmodes with $q_1^2 > 0$ and $q_2^2 < 0$ are the bulk-surface electromagnetic waves, whereas the eigenmodes with $q_1^2 < 0$ and $q_2^2 < 0$ are the surface electromagnetic waves.

For the bulk-surface eigenmodes, the spectral components of the electromagnetic field, $E_{zn}(\rho, q_z, \omega)$ and $H_{zn}(\rho, q_z, \omega)$, have the forms

$$E_{zn}(\rho, q_z, \omega) = A_n^E J_n(q_1 \rho),$$
$$H_{zn}(\rho, q_z, \omega) = A_n^H J_n(q_1 \rho) \quad (12)$$

for the cylinder region ($\rho \leqslant \rho_c$, $q_1^2 > 0$), and

$$E_{zn}(\rho, q_z, \omega) = B_n^E K_n(|q_2| \rho),$$
$$H_{zn}(\rho, q_z, \omega) = B_n^H K_n(|q_2| \rho) \quad (13)$$

for the vacuum region ($\rho \geqslant \rho_c$, $q_2^2 < 0$). Here $J_n(u)$ is the nth-order Bessel function of the first kind, and $K_n(u)$ is the nth-order modified Bessel function of the second kind (Macdonald function) (see Ref. [32]); $A_n^{E,H}$ and $B_n^{E,H}$ are the arbitrary constants.

The spectral components of the electromagnetic field for the surface eigenmodes are described by the same Eqs. (12) and (13) as for bulk-surface waves, where, however, we take a modified Bessel function of the first kind, $I_n(u)$ (the Infeld function), instead of the Bessel function $J_n(u)$ because inside the cylinder the condition $q_1^2 < 0$ holds. The choice of solutions is conditioned by the demand to fulfill the requirements of finiteness of the values $E_{zn}(\rho, q_z, \omega)$ and $H_{zn}(\rho, q_z, \omega)$ at $\rho \to 0$ and $\rho \to \infty$.

Other Fourier components of electromagnetic fields inside ($\rho < \rho_c$) and outside ($\rho > \rho_c$) the cylinder are expressed via values $E_{zn}(\rho, q_z, \omega)$ and $H_{zn}(\rho, q_z, \omega)$ using Maxwell's equations. Note that, for the nonzero azimuthal mode indices, the eigenmodes under study are hybrid ones, i.e., these eigenmodes have all components of the electric and magnetic fields.

We represent the surface current $\vec{j}_\tau^{2D}(\varphi, z, t)$ in the form

$$\vec{j}_\tau^{2D}(\varphi, z, t) = \sum_{n=-\infty}^{\infty} \int_{-\infty}^{\infty} \int_{-\infty}^{\infty} \vec{j}_{\tau n}^{2D}(q_z, \omega) \times \exp[i(q_z z + n\varphi - \omega t)] dq_z d\omega, \quad (14)$$

where

$$j_{\alpha n}^{2D}(q_z, \omega) = \sum_\beta \sigma_{\alpha\beta}(n, q_z, \omega) E_{\beta n}(q_z, \omega). \quad (15)$$

$\sigma_{\alpha\beta}(n, q_z, \omega)$ ($\alpha, \beta = \varphi, z$) are the tensor components of the nanotube conductivity, the general expressions for which were derived in Ref. [33].

Using Eqs. (10), (15), and the continuity equation (6), we find the following expression for the Fourier component of the surface density of charge carriers in the nanotube:

$$n^{2D}(n, q_z, \omega) = \frac{q_z}{e\omega} \sum_\beta \left[\frac{n}{q_z \rho_c} \sigma_{\varphi\beta}(n, q_z, \omega) + \sigma_{z\beta}(n, q_z, \omega) \right] E_{\beta n}(\rho_c; q_z, \omega), \quad (16)$$

where $\beta = \varphi, z$. Satisfying the above boundary conditions on the cylinder surface, we obtain the dispersion equation for the eigenmodes spectra for the semiconductor nanotube with a dielectric filling,

$$\Delta(n, q_z, \omega) = \frac{4\pi i}{\omega \rho_c} \left[\frac{n^2}{\rho_c^2 q^2} \sigma_{\varphi\varphi}(n, q_z, \omega) + \sigma_{zz}(n, q_z, \omega) \right] \times \Delta^H(n, q_z, \omega), \quad (17)$$

where

$$\Delta(n, q_z, \omega) = \Delta^E(n, q_z, \omega)\Delta^H(n, q_z, \omega) - \Delta_0(n, q_z, \omega), \tag{18}$$

$$\Delta^E(n, q_z, \omega) = \frac{1}{q\rho_c}\frac{K_n'(q\rho_c)}{K_n(q\rho_c)} + \frac{\varepsilon}{q_1\rho_c}\frac{J_n'(q_1\rho_c)}{J_n(q_1\rho_c)}, \tag{19}$$

$$\Delta^H(n, q_z, \omega) = \frac{1}{q\rho_c}\frac{K_n'(q\rho_c)}{K_n(q\rho_c)} + \frac{1}{q_1\rho_c}\frac{J_n'(q_1\rho_c)}{J_n(q_1\rho_c)}, \tag{20}$$

$$\Delta_0(n, q_z, \omega) = \left[\frac{n\omega q_z(\varepsilon - 1)}{q_1^2 q^2 \rho_c^2 c}\right]^2, \tag{21}$$

with $q = \sqrt{-q_2^2} = \sqrt{q_z^2 - \omega^2/c^2}$. Here the prime denotes the derivative of the corresponding special function with respect to its argument.

In the absence of a semiconductor nanotube, the relation $\Delta(n, q_z, \omega) = 0$ for $n \geqslant 1$ can be interpreted as the dispersion equation for hybrid E- and H-type waves. The symmetric ($n = 0$) cylindrical E-type eigenmodes are characterized by the dispersion relation $\Delta^E(0, q_z, \omega) = 0$, whereas the symmetric H-type waves are characterized by equation $\Delta^H(0, q_z, \omega) = 0$. Note that the special case of dispersion equation (17) in the quasistationary approximation (when $c \to \infty$) and for $\varepsilon = 1$ was derived in Ref. [28]. In this case, it describes slow surface hybrid eigenmodes in a hollow semiconductor nanotube.

To determine the type of hybrid waves, we introduce the following value:

$$\Re = \frac{|E_{zn}(\rho, q_z, \omega_g)|_{\max}}{|H_{zn}(\rho, q_z, \omega_g)|_{\max}},$$

where the index "max" indicates the maximum value of the corresponding component. For hybrid E- and H-type waves, the conditions $\Re > 1$ and $\Re < 1$ are satisfied, respectively. From these facts, it transpires that the wave type is determined by the dominant axial component of the electromagnetic field [34]. The mode subscript g represents actually two indexes, the azimuthal number n and the radial number s, which is the number of field variations along the radial coordinate. In the case of symmetric waves, the index s corresponds to the root number of the corresponding dispersion equation: $\Delta^E(0, q_z, \omega) = 0$ or $\Delta^H(0, q_z, \omega) = 0$. In the dispersion equation $\Delta(n, q_z, \omega) = 0$, the role of the coupling factor between the E- and H-waves is played by the quantity $\Delta_0(n, q_z, \omega)$. If $n = 0$, the dispersion equation $\Delta(n, q_z, \omega) = 0$ splits into two independent equations, $\Delta^E(0, q_z, \omega) = 0$ and $\Delta^H(0, q_z, \omega) = 0$. In this case, the electromagnetic fields of symmetric waves have three components: $E_{\rho 0s}, H_{\varphi 0s}$, and E_{z0s} for E waves, and $H_{\rho 0s}, E_{\varphi 0s}, H_{z0s}$ for H waves. If $n \neq 0$, all electric and magnetic field components of the cylindrical eigenmodes are nonzero, and, therefore, they are the hybrid E- and H-type waves. In Refs. [34,35], a method was provided for the separation of such modes into the so-called HE_{ns} and EH_{ns} modes depending on the predominant axial component of the electromagnetic field. If the axial component of the electric field dominates ($\Re > 1$), the eigenmode is the HE_{ns} mode (of E type); otherwise it is the EH_{ns} mode (of H type).

Note that the inclusion of a semiconductor nanotube in the system under consideration does not violate the symmetry of the problem. Therefore, the above-described classification of eigenmodes is also suitable for the system with a nanotube. For the conductivity tensor components of a semiconductor nanotube, we use the expressions obtained in Ref. [33]. We write below only components needed for our analysis. These are as follows:

$$\mathrm{Re}\,\sigma_{\varphi\varphi}(n, q_z, \omega) = -\frac{e^2}{4\pi m^* |q_z| \rho_c^3 \omega} \sum_{m'} \left\{ \left(m' + \eta + \frac{n}{2}\right)^2 [\theta(A_{+-+}) - \theta(A_{---+})] - \left(m' + \eta - \frac{n}{2}\right)^2 [\theta(A_{++-}) - \theta(A_{-+-})] \right\}, \tag{22}$$

$$\mathrm{Re}\,\sigma_{zz}(n, q_z, \omega) = -\frac{e^2}{8\pi \varepsilon_0 |q_z|^3 \rho_c^3 \omega} \sum_{m'} \{(\omega - \Omega_+)^2 [\theta(A_{+-+}) - \theta(A_{---+})] - (\omega - \Omega_-)^2 [\theta(A_{++-}) - \theta(A_{-+-})]\}, \tag{23}$$

$$\mathrm{Im}\,\sigma_{\varphi\varphi}(n, q_z, \omega) = \frac{e^2 n_0^{2D}}{m^* \omega} \left\{ 1 - \frac{1}{4\pi^2 n_0^{2D} \rho_c^3 q_z} \sum_{m'} \left[\left(m' + \eta + \frac{n}{2}\right)^2 \ln \left|\frac{A_{+-+}}{A_{---+}}\right| - \left(m' + \eta - \frac{n}{2}\right)^2 \ln \left|\frac{A_{++-}}{A_{-+-}}\right| \right] \right\}, \tag{24}$$

$$\mathrm{Im}\,\sigma_{zz}(n, q_z, \omega) = -\frac{e^2 n_0^{2D}}{m^* \omega q_z^2 \rho_c^2} \left\{ n^2 + \frac{\hbar^2}{16\pi^2 n_0^{2D} \rho_c^3 q_z \varepsilon_0^2} \sum_{m'} \left[(\omega - \Omega_+)^2 \ln \left|\frac{A_{+-+}}{A_{---+}}\right| - (\omega - \Omega_-)^2 \ln \left|\frac{A_{++-}}{A_{-+-}}\right| \right] \right\}. \tag{25}$$

Here $\theta(u)$ is the Heaviside theta function, m^* is the electron effective mass, n_0^{2D} is the equilibrium surface electron density, $\hbar$ is the Planck constant, η is the number Φ/Φ_0 of magnetic flux quanta $\Phi_0 = 2\pi\hbar c/e$ inside the nanotube,

$$A_{+-+} = q_z v_{m'} - \omega_- + \Omega_+,$$
$$A_{---+} = -q_z v_{m'} - \omega_- + \Omega_+,$$
$$A_{++-} = q_z v_{m'} - \omega_+ + \Omega_-,$$
$$A_{-+-} = -q_z v_{m'} - \omega_+ + \Omega_-,$$
$$v_m = \sqrt{\frac{2}{m^*}(\epsilon_F - \epsilon_m)} \tag{26}$$

is the maximum value of electron velocity along the tube axis in subzone with boundary energy $\epsilon_m = \epsilon_0(m + \eta)^2$, $\epsilon_0 = \hbar^2/2m^*\rho_c^2$ is the rotational quantum, $m = 0, \pm 1, \ldots$ is the quantum number defining the z-projection of electron angular momentum $m\hbar$, ϵ_F is the Fermi energy which is related to the

electron density n_0^{2D} in the nanotube by the equation

$$n_0^{2D} = \frac{\sqrt{2m^*}}{2\pi^2\hbar\rho_c}\sum_m \sqrt{\epsilon_F - \epsilon_m}$$
$$= \frac{1}{2\pi^2\rho_c^2}\sum_m \sqrt{\frac{\epsilon_F}{\epsilon_0} - (m+\eta)^2},$$
$$\omega_\pm = \omega \pm \hbar q_z^2/2m^*,$$
$$\Omega_\pm(n, m') = \frac{\epsilon_0}{\hbar}[\pm(m' + \eta \pm n)^2 \mp (m' + \eta)^2] \qquad (27)$$

is the frequency of the "vertical" electron transitions between subzones of the electron spectrum in the nanotube (see Ref. [33]). The summation over m in Eqs. (22)–(25) and (27) is done from $m_{\min}$ to $m_{\max}$, where $m_{\min}$ and $m_{\max}$ are the minimal and maximal values of m satisfying the condition $\epsilon_F > \epsilon_m$. In Eqs. (22)–(25), we neglect the spin level splitting because we consider the semiconductor materials with small effective masses, $m^* \ll m_0$ (see Ref. [33]), where m_0 is the mass of a free electron.

It might be worthwhile to point out that the tensor components Eqs. (22)–(25) of conductivity were obtained in Ref. [33] without taking into account the collisions of charge carriers in the nanotube, but with regard to the electron transitions between the valence and conductivity zones. Only these transitions provide the real components Eqs. (22) and (23) of the conductivity tensor. These real components of the conductivity are nonzero in a very narrow range of frequencies with relative width of the order of $v_F/c \ll 1$, where v_F is the Fermi velocity of electrons in the semiconductor. We assume that the electron collisions in the nanotube make a more significant contribution to the real part of the conductivity tensor and affect the behavior of the eigenmode spectrum of the structure under consideration. Taking these comments into account, we use Eqs. (24) and (25) below for the conductivity tensor components, where we replace, however, frequency ω by $\omega + i\nu$. Here ν is the collision frequency. In doing so, these components become complex, and later we omit the symbol "Im" for them.

B. Analysis of the eigenmodes spectrum

It is convenient to carry out the analysis of the eigenmodes spectrum using the dimensionless frequency $\Omega = \omega/\omega_0$ and wave number $Q = q_z\rho_c$ with $\omega_0 = c/\rho_c$. In the numerical calculations, we choose the following geometric and material parameters of the structure: $\rho_c = 50$ nm, $\varepsilon = 9.8$ (for policor dielectric), and $m^* = 0.013\ m_0$ (for InSb semiconductor). For these parameters, we have $\omega_0 = 6 \times 10^{15}$ s^{-1} and $\epsilon_0 \approx 1.16$ meV. The value of magnetic field which corresponds to the magnetic flux quanta Φ_0 is $B_0 \approx 0.525$ T. According to Ref. [27], the radius of a semiconductor nanotube can reach 200 nm, which gives $B_0 \approx 0.138$ T. For a chosen value of $\rho_c = 50$ nm, the peculiarities of the eigenmodes spectrum discussed below arise in the terahertz frequency range. Numerical calculations show that the greater the radius ρ_c, the fewer the frequencies where these peculiarities take place.

The analysis of the spectra of the bulk-surface electromagnetic eigenmodes in the dielectric cylinder was presented in Refs. [36]. In Ref. [30], we have shown that, in the collisionless regime, the spatial dispersion of nanotube conductivity causes the splitting of the dispersion curves for the nonsymmetrical (hybrid) eigenmodes. This splitting takes place only for the modes with one variation of fields by radius. This is due to the fact that the frequency region in which the splitting occurs is well below the frequencies of other modes. A very interesting fact is that the number of split eigenmode branches oscillates when changing the number of magnetic flux quanta in the nanotube. In addition, the frequencies of these modes also oscillate with the same period. These oscillations are caused by corresponding oscillations of the nanotube conductivity, and they are manifestations of the Aharonov-Bohm effect. The latter, in turn, occur as a result of oscillations of the number of subzones in the electron energy spectrum of the nanotube when the number of magnetic flux quanta changes.

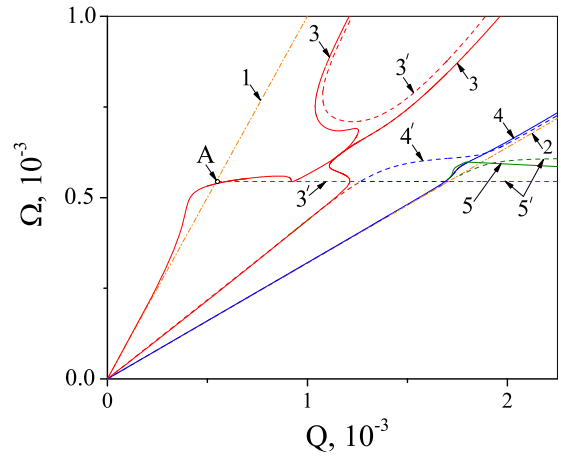

FIG. 2. Dispersion curves for eigenmodes in the collisionless regime ($\nu = 0$, dashed curves 3′, 4′, and 5′) and taking into account the relaxation frequency $\nu = 3 \times 10^{11}$ s^{-1} (solid curves 3, 4, and 5) built using the numerical solution of the dispersion equation (17). Red curves 3 and 3′ correspond to nonsymmetrical (hybrid) bulk-surface HE_{11} waves (i.e., E type modes) with $n = s = 1$, while blue curves 4 and 4′ are for EH_{11} modes (i.e., H type modes). Green curves 5′ and a pair of closely spaced dashed curves 5 are for the surface waves. Dash-dotted orange lines 1 and 2 correspond to the vacuum ($\Omega = Q$) and dielectric ($\Omega = Q/\sqrt{\varepsilon}$) light lines. Letter A denotes the point of intersection of solid red dispersion curve 3 and the vacuum light line 1. Note that point A is located at the starting point of the dispersion curve 3′. The values of the parameters are $n_0^{2D} = 5.35 \times 10^{13}$ m^{-2}, $\epsilon_F \approx 2.33$ meV, $\eta = 1.42$, and m in Eqs. (24) and (25) takes on the values $-2, -1$.

Here we discuss the changes in the eigenmodes spectrum due to the electron collisions in the nanotube. Figure 2 demonstrates these changes for nonsymmetrical (hybrid) bulk-surface waves with $n = s = 1$ and for the surface waves. The dispersion curves are built using the numerical solution of the dispersion equation (17) without taking into account the electron relaxation frequency ($\nu = 0$, dashed curves 3′, 4′, and 5′) and for $\nu = 3 \times 10^{11}$ s^{-1} (solid curves 3, 4, and 5).

As seen from Fig. 2, the electron collisions result in significant restructuring of the eigenmodes spectrum. At first glance, it may seem unexpected that taking into account the relatively small relaxation frequency ($\nu/\omega \ll 1$) leads to such a significant rearrangement of the eigenmode spectrum.

However, one should pay attention to the fact that, as is clearly seen in Fig. 2, this *significant restructuring spectrum* occurs at *very insignificant changes in the eigenmode frequencies* by the values $\Delta\Omega$ of the order of ν. Such changes of the eigenmode frequencies are quite expected.

The most important change consists in the appearance of a section in dispersion curve 3 located to the left of the vacuum light line 1. The phase velocities of the waves corresponding to this section are greater than the velocity of light in the vacuum. The electromagnetic waves of the electric type (*TM*-type), propagating along the flat metal-dielectric interface with phase velocities greater than the velocity of light in the vacuum, are referred to as Zenneck's waves [31], while the *E*-type waves propagating along cylindrical conductors in a dielectric environment were named Sommerfeld's waves [37,38].

A detailed analysis of the dispersion curves for surface polaritons and Zenneck's waves at the flat air-germanium interface was performed in Ref. [39]. It was shown, in particular, that there are so-called crossover points at the intersections of the dispersion curves with the vacuum light line. To the left of these points, the dispersion curves correspond to Zenneck's waves, while to the right of these points the dispersion curves are for the surface polaritons. In our case, the crossover point is point A in Fig. 2. Note that unlike the well-known Zenneck-Sommerfeld's supraluminal waves, the waves that we describe (curve 3 in Fig. 2) are hybrid HE_{n1}-type waves. Despite their hybrid nature, the supraluminal waves considered here are *E*-type modes, like the Zenneck-Sommerfeld waves. Similar to the Zenneck-Sommerfeld waves, HE_{n1}-type supraluminal waves in conductive nanotubes may be of interest for use in nanoscale terahertz transmission lines (see, e.g., [40–42]).

Strictly speaking, the supraluminal waves similar to Zenneck-Sommerfeld's waves are not eigenmodes of the system because they have a nonzero radial component of the Poynting vector in the vacuum directed away from the sample surface. However, the wave leakage into vacuum can be considered as an additional source of mode damping, along with Joule losses. Therefore, we can continue to consider Zenneck-Sommerfeld's and similar waves as eigenmodes with two sources of their damping.

The analysis of the dispersion equation (17) shows that taking into account the electron collisions in the nanotube does not result in the appearance of supraluminal portions of the dispersion curves for the azimuthally symmetric modes but only for the nonsymmetrical hybrid HE_{n1} modes (i.e., for *E* type modes) only.

In Ref. [30], the following dependence of the number $N_{\rm BSW}$ of split spectrum branches for the hybrid eigenmodes on the number k of filled electronic energy subzones was established: $N_{\rm BSW} = 2|2k-1|+1$. The number k changes in a jump $\Delta k = -1$ when the value of magnetic flux satisfies the condition $\eta = j + \sqrt{\epsilon_F/\epsilon_0}$ (where j is integer number). Reversal jumps occur at $\eta = j - \sqrt{\epsilon_F/\epsilon_0}$. The electron collisions in the nanotube result in the merging of the spectral branches (i.e., in the disappearance of gaps in the spectrum by frequency) and a greater difference in the wave number Q of the dispersion curves near the turning point of the spectrum. Therefore, it is more correct to say that the number $N_{\rm ND}$ of sections of dispersion curves with negative dispersion increases when the number k of filled electronic subzones increases. The value of $N_{\rm ND}$ oscillates when changing the number of magnetic flux quanta in the nanotube, similarly to the oscillations of $N_{\rm BSW}$ in the absence of collisions [30]. The splitting of the dispersion curves for the EH_{ns} waves is less pronounced than that for the HE_{ns} modes.

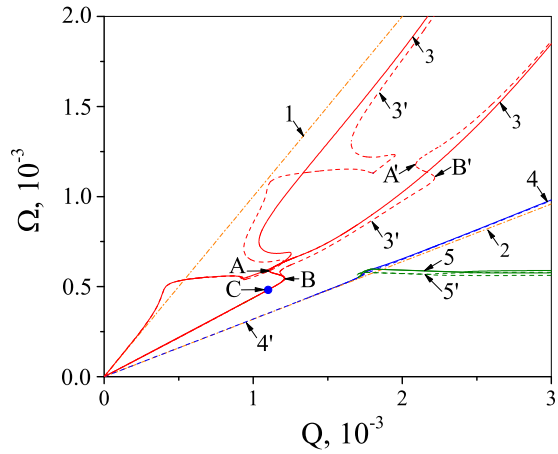

FIG. 3. Dispersion curves for the eigenwaves in a semiconductor nanotube with dielectric filling at different values of the magnetic flux. Solid curves 3, 4, and 5 are plotted for $\eta = 1.42$ (slightly above the critical value $\eta_{\rm cr} = \sqrt{\epsilon_F/\epsilon_0} = \sqrt{2}$). These curves are the same as curves 3, 4, and 5 in Fig. 2. Dashed curves 3′, 4′, and 5′ correspond to $\eta = 1.41$ (slightly below the critical value $\eta_{\rm cr}$). Points A,B and A', B' indicate the characteristic sections of the dispersion curves where the normal dispersion changes by the anomalous one. The behavior of point C on dispersion curve 3 when increasing magnetic flux is followed in Fig. 5.

Figure 3 shows the dispersion dependences for the eigenmodes in a semiconductor nanotube with the dielectric filling for $\epsilon_F \approx 2.33$ meV ($\epsilon_F/\epsilon_0 = 2$), $\nu = 3\times10^{11}$ s^{-1}, and the following two values of filling factor η: $\eta = 1.41 < \eta_{\rm cr} = \sqrt{2}$ ($m = -2, -1, 0$, $k = 3$, dashed curves 3′, 4′, and 5′) and $\eta = 1.42 > \eta_{\rm cr}$ ($m = -2, -1$, $k = 2$, solid curves 3, 4, and 5). Points A,B and A', B' indicate the characteristic sections of the dispersion curves where the derivative $d\Omega/dQ$ tends to infinity, and normal dispersion changes by an anomalous one.

It is evident from Fig. 3 that the number of sections with negative dispersion in curve 3′ (which corresponds to $k = 3$ and $m = -2, -1, 0$) is larger than that in curve 3 (with $k = 2$ and $m = -2, -1$). The sections with negative dispersion in curves 4 and 4′ are much less pronounced than that on curves 3 and 3′.

It should be noted that turning points such as A,B in curve 3 and A', B' in curve 3′ appear due to the specific features of the frequency and spatial dispersion of the conductivity tensor components in the regions of Q and Ω where new subzones of the electron energy spectrum arise. Figure 4 demonstrates the peculiarities of the real and imaginary parts of the conductivity tensor components $\bar{\sigma}_{\varphi\varphi}(n, Q, \Omega)$ in the vicinity of turning points A and B on curve 3 in Fig. 3. Here the values $\mathrm{Re}\,\sigma_{\varphi\varphi}(n, Q, \Omega)$ and $\mathrm{Im}\,\sigma_{\varphi\varphi}(n, Q, \Omega)$ are expressed in units of $\sigma_0 = e^2 n_0^{2D}/m^*\omega_0$. As seen from Fig. 4, the characteristic bends of the dependences $\mathrm{Re}\,\bar{\sigma}_{\varphi\varphi}(n, Q, \Omega)$ appear at points corresponding to the turning points on the dispersion curve 3 in Fig. 3.

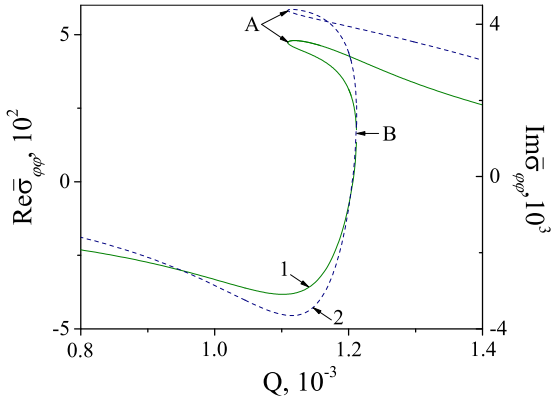

FIG. 4. Dependences of the real (solid curve 1) and imaginary (dashed curve 2) parts of the conductivity tensor component $\bar{\sigma}_{\varphi\varphi}(n, Q, \Omega)$ on the wave number Q in the vicinity of turning points A and B on the dispersion curve 3 in Fig. 3.

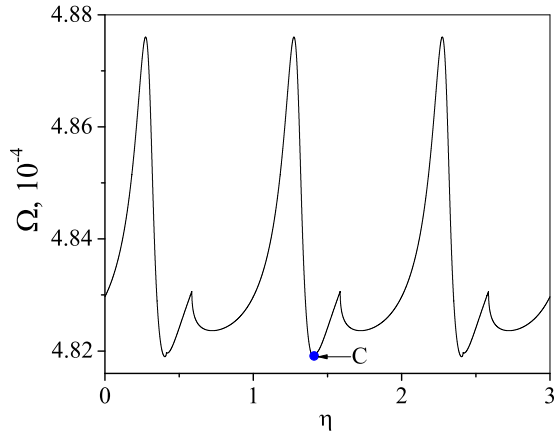

FIG. 5. Dependence $\Omega(\eta)$ for the HE_{11} bulk-surface wave at $Q = 1.1 \times 10^{-3}$. Point C at $\eta = 1.42$ corresponds to point C in Fig. 3.

When looking at Fig. 4, it might give the impression that the real and imaginary parts of the conductivity tensor component $\bar{\sigma}_{\varphi\varphi}(n, Q, \Omega)$ are multivalued functions of the wave vector Q. Meanwhile, as is evident from Eq. (24), $\bar{\sigma}_{\varphi\varphi}(n, Q, \Omega)$ is a single-valued function of two arguments, of the wave vector Q and of the frequency Ω. It should be noted that when constructing the dependences of $\mathrm{Re}\,\sigma_{\varphi\varphi}$ and $\mathrm{Im}\,\sigma_{\varphi\varphi}$ on the wave vector Q, shown in Fig. 4, we do not consider the frequency Ω as an independent argument but take it from the solution of dispersion equation (17). Since there exist several dispersion curves $\Omega(Q)$ in the vicinity of turning points A and B (see Fig. 3), we have several values of Ω that correspond to the same value of Q and, correspondingly, several values of the conductivity tensor components.

The dependences of the real and imaginary parts of the conductivity tensor components $\bar{\sigma}_{zz}(n, Q, \Omega)$ on Q near the turning points of the spectrum, like A,B and A', B', have similar features.

It is of interest to follow the behavior of the dispersion curves when changing the magnetic flux through the nanotube. In the quasistationary approximation, the Aharonov-Bohm oscillations of plasmon frequency in a hollow semiconducting nanotube were studied in Ref. [28]. Here, as an example, we choose the point C (marked with a filled circle) on the dispersion curve 3 in Fig. 3 for the HE_{11} bulk-surface wave at $Q = 1.1 \times 10^{-3}$. Figure 5 demonstrates the Aharonov-Bohm oscillations of the eigenmode frequency when increasing the magnetic flux.

III. WAVE EXCITATION BY CHARGED PARTICLES

The total radiative energy loss of the electron can be estimated by determining the work done by the wave electric field being excited by the moving electron per unit time,

$$\frac{dW}{dt} = evE_z(\rho_e, \varphi_e, vt; t), \tag{28}$$

where $E_z(\rho_e, \varphi_e, vt; t)$ is the z-component of the electric field excited by the moving electron at the electron location point, i.e., at point $(\rho = \rho_e, \varphi = \varphi_e, z = vt)$.

By representing the function $n_e(\vec{r}, t)$ in cylindrical coordinates as (see Ref. [43])

$$n_e(\vec{r}, t) = \frac{\delta(\rho - \rho_e)}{\sqrt{\rho\rho_e}}\delta(\varphi - \varphi_e)\delta(z - vt), \tag{29}$$

we obtain the corresponding solutions of the Maxwell equations for the Fourier components of the electric field of the moving electron. Then, using the boundary conditions discussed above and Eq. (28), we find the following expression for the electron energy loss per unit time [30]:

$$\frac{dW}{dt} = -\frac{e^2}{\rho_c}\sum_{n=-\infty}^{\infty}\frac{K_n^2(\rho_e|q_z|)I_n(\rho_c|q_z|)\Delta^H(n, q_z, \omega_g)}{K_n(\rho_c|q_z|)|\Delta'(n, \omega/v, \omega)|_{\omega_g}} \times\left[\frac{\varepsilon}{q_1\rho_c}\frac{J_n'(\rho_c q_1)}{J_n(\rho_c q_1)} + \frac{|q_z|}{q_z}\frac{I_n'(\rho_c|q_z|)}{I_n(\rho_c|q_z|)}\right], \tag{30}$$

where $q_z = \omega_g/v$, i.e., the fulfillment of the Cherenkov resonance condition is taken into account, ω_g is the frequency of the cylinder eigenmode satisfying the dispersion equation $\Delta(n,\ q_z = \omega_g/v,\ \omega_g) = 0$, and the value $|\Delta'(n, \omega/v, \omega)|_{\omega_g}$ is the modulus of the first derivative of $\Delta(n, q_z = \omega/v, \omega)$ with respect to ω taken at $\omega = \omega_g$.

As noted above, the dispersion curves for both the bulk-surface and surface waves have parts with negative dispersion. This means that the structure under study can be used as materials for constructing both the generators and amplifiers of electromagnetic radiation. Indeed, this is possible under propagation of the tubular flow of electrons along the structure when the beam instability effect emerges. The electrons in beams, as a rule, have a certain spread in velocity, so the kinetic instability occurs when the electron velocity variation exceeds some critical value (see, e.g., Ref. [44]),

$$\frac{|\Delta\vec{u}|}{|\vec{u}|} > \frac{|\omega - q_z v_0|}{q_z v_0}. \tag{31}$$

Here $\vec{u}$ is an electron velocity in the flow, $\Delta\vec{u}$ is the velocity variation, and v_0 is the directed motion velocity of the flow.

An important characteristic of the beam instability is the increment γ. Recall that the instability increment characterizes the exponential growth of the wave amplitude (or intensity)

at the linear stage of the instability development (see, e.g., Ref. [44]). In this paper, we study the amplitude instability in time of the waves in the structure under consideration when they interact with the electron beam. In this case, the increment has a frequency dimension, and its inverse value indicates how long it takes for the wave amplitude to increase by e times. To obtain the increment of the kinetic instability, we use the so-called energy approach, following Ref. [45]. The essence of this approach is to represent the energy of the excited waves in the form of a sum of quanta $\hbar\omega_g$ of elementary excitations, the change of the number $\aleph_g$ of which is described by the corresponding kinetic equation,

$$\frac{\partial \aleph_g}{\partial t} = \frac{2\pi}{\hbar}\sum_{\vec{k}_1,\vec{k}_2} \left|W_{\vec{k}_1,g,\vec{k}_2}\right|^2 \delta(\Theta_1 - \Theta_2 - \hbar\omega_g) \times \left[(\aleph_g + 1)n_{\vec{k}_1}\left(1 - n_{\vec{k}_2}\right) - \aleph_g n_{\vec{k}_2}\left(1 - n_{\vec{k}_1}\right)\right], \quad (32)$$

$$\sum_g \hbar\omega_g \frac{\partial \aleph_g}{\partial t} = \frac{1}{4\pi}\int\left(\vec{H}\frac{\partial \vec{H}}{\partial t} + \vec{E}\frac{\partial \vec{D}}{\partial t}\right)d\vec{r} = -\frac{dW}{dt}, \quad (33)$$

where $n_{\vec{k}_j} = (0, 1)$ is the occupation number of the electron quantum state with wave vector k_j, $\Theta_j = \hbar^2 k_j^2/2m_0$ is the energy of an electron in the state with wave vector k_j, $W_{\vec{k}_1,g,\vec{k}_2}$ is the Hamiltonian matrix element of the electron interaction with the electromagnetic field quantum with energy $\hbar\omega_g$, and integration in Eq. (33) is done over the volume occupied by the field of excited eigenmodes.

The energy loss of a single electron per unit time can be considered as the power of spontaneous radiation. So, when calculating $|W_{\vec{k}_1,g,\vec{k}_2}|^2$, we should put $\aleph_g \to 0$, $n_{\vec{k}_2} \to 0$, $n_{\vec{k}_1} \to 1$. Substituting Eq. (32) into Eq. (33) and comparing the result with Eq. (30), we get

$$\left|W_{\vec{k}_1,g,\vec{k}_2}\right|^2 = \frac{e^2\hbar v}{L\rho_c}\frac{K_n^2(\rho_e|q_z|)I_n(\rho_c|q_z|)\Delta^H(q_z,\omega_g,n)}{\omega_g K_n(\rho_c|q_z|)|\Delta'(n,q_z,\omega)|_{\omega_g}} \times \left[\frac{\varepsilon}{q_1\rho_c}\frac{J_n'(\rho_c q_1)}{J_n(\rho_c q_1)} + \frac{|q_z|}{q_z}\frac{I_n'(\rho_c|q_z|)}{I_n(\rho_c|q_z|)}\right]. \quad (34)$$

Here q_1 is taken at $\omega = \omega_g$, $\Delta'(n, q_z, \omega)|_{\omega_g}$ is the first derivative of $\Delta(n, q_z, \omega)$ with respect to ω taken at ω_g, and L is the characteristic length of the localization of the fields in the vacuum along the cylinder radius. The product of matrix element square $|W_{\vec{k}_1,g,\vec{k}_2}|^2$ and $(2\pi/\hbar)\delta(\Theta_1 - \Theta_2 - \hbar\omega_g)$ determines the probability of the electron transition from the state Θ_2 with the wave vector $\vec{k}_2$ into the state Θ_1 with the wave vector $\vec{k}_1$ with absorption of the plasmon with energy $\hbar\omega_g$ in the time unit [45].

Contrary to the radiation of a single electron, the radiation of the beam of charged particles is defined by the induced processes. Using Eq. (32) and taking into account the smallness of momentum $\hbar q_z$ of the electromagnetic field quantum compared to the electron momentum $\hbar k_z$, we find the expression for the increment γ of the studied modes when they interact with the electron beam. At electron temperatures (expressed in energy units) $T > \hbar\omega_g$, we have

$$\gamma = \frac{1}{\aleph_g}\frac{\partial \aleph_g}{\partial t} = \frac{2\pi V}{\hbar} \times \int \left|W_{\vec{k}_1,g,\vec{k}_2}\right|^2 \delta\left(u_z - \frac{\omega_g}{q_z}\right)\frac{\partial f(\vec{p})}{\partial p_z}d\vec{p}, \quad (35)$$

where $\vec{p} = \hbar\vec{k}$ is the momentum of the beam electron, V is the localization volume of fields in the vacuum, $f(\vec{p})$ is the Maxwell distribution function

$$f(\vec{p}) = \frac{n_0^B}{(2\pi m_0 T)^{3/2}}\exp\left[-\frac{(p_z - p_0)^2 + p_\varphi^2 + p_\rho^2}{2m_0 T}\right], \quad (36)$$

and n_0^B and $p_0 = m_0 v_0$ are the equilibrium electron density and the directed motion momentum of the flow. We emphasize that the wave vector of the beam electron $\vec{k} = \vec{p}/\hbar$ is precisely the value that is used in the definition of the matrix element $W_{\vec{k}_1,g,\vec{k}_2}$. We note also that, when substituting Eq. (34) into Eq. (35), we should replace the value v by p_z/m_0.

Performing the integration in Eq. (35), we get the following expression for the increment:

$$\gamma = \frac{e^2 S n_0^B\sqrt{2\pi m_0}}{T^{3/2}\rho_c q_z}\frac{K_n^2(\rho_e|q_z|)I_n(\rho_c|q_z|)\Delta^H(q_z,\omega_g,n)}{K_n(\rho_c|q_z|)|\Delta'(n,q_z,\omega)|_{\omega_g}} \times \left[\frac{\varepsilon}{q_1\rho_c}\frac{J_n'(\rho_c q_1)}{J_n(\rho_c q_1)} + \frac{|q_z|}{q_z}\frac{I_n'(\rho_c|q_z|)}{I_n(\rho_c|q_z|)}\right]\left(v_0 - \frac{\omega_g}{q_z}\right) \times \exp\left[-\frac{m_0}{2T}\left(v_0 - \frac{\omega_g}{q_z}\right)^2\right], \quad (37)$$

where $S \sim 1/q^2$ is the square of the localization region of the fields in the vacuum in plane perpendicular to the cylinder axis. As follows from Eq. (37), the increment is positive ($\gamma > 0$) at $v_0 > \omega_g/q_z$. This means that the beam instability occurs and the electromagnetic waves are excited by the beam.

IV. NUMERICAL ANALYSIS OF WAVE EXCITATION

For the correct numerical analysis of both the electron energy loss and the beam instability increment, it is necessary to take into account the dissipative loss of the excited waves through taking into account the electron collisions in the nanotube.

A. Electron energy loss

In this subsection, we perform a numerical analysis of the dependence of the electron energy loss [Eq. (30)] on the number of flux quanta η for the following parameter values: $\beta = 0.33$, $Q = 1.79 \times 10^{-3}$, $\epsilon_F/\epsilon_0 = 2$, $\rho_e = 1.1\rho_c$, $\nu = 3 \times 10^{11}$ s^{-1}; the value k changes from 2 [$m = -2$, -1 and $\eta \in (0.415; 0.59)$ with period 1] to 3 [$m = -2$, -1, 0 and $\eta \in (0.59; 1.415)$ with period 1].

According to Eq. (30), the electron energy loss occurs due to the excitation of the waves satisfying the Cherenkov resonance condition, $\omega = q_z v$. This means that the discrete set of points (Q, Ω) lying on the intersections of the all dispersion curves and the line $\Omega = \beta Q$ define the waves responsible for the energy loss of the electron moving with the velocity $v = \beta c$. The chosen parameter β corresponds to the electron

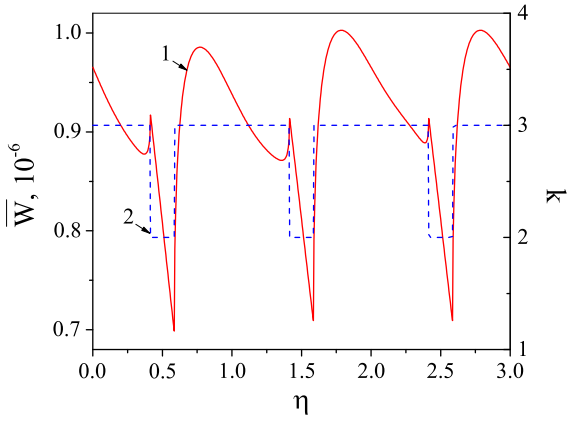

FIG. 6. Aharonov-Bohm oscillations of the dimensionless loss $\overline{W} = -(dW/dt)/(dW/dt)_0$ (red solid curve 1) due to the excitation of the EH_{11} bulk-surface wave and of the number k of filled electron energy subzones (blue dashed curve 2).

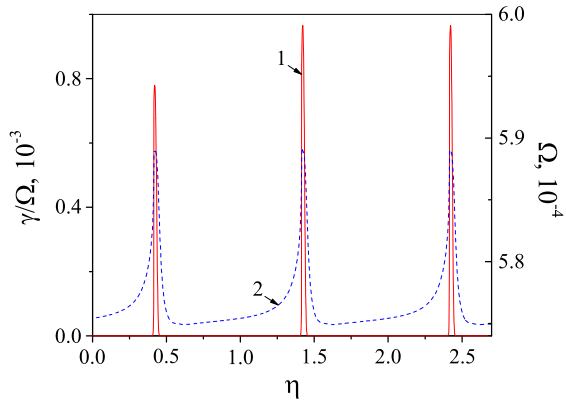

FIG. 7. Dependence of the relative increment γ/Ω of the kinetic instability due to the excitation of EH_{11} bulk-surface waves on the number η of the magnetic flux quanta (solid red curve 1) and the dependence $\Omega(\eta)$ (dashed blue curve 2) for $Q = 1.79 \times 10^{-3}$, $\rho_e = 1.1\rho_c$, $\nu = 3 \times 10^{11}$ s^{-1}. The value k of the electron energy subzones in nanotube changes from 2 [$m = -2, -1$ and $\eta \in (0.415; 0.59)$ with period 1] to 3 [$m = -2, -1, 0$ and $\eta \in (0.59; 1.415)$ with period 1].

velocity v that is higher than the light velocity $c/\sqrt{\varepsilon}$ in the dielectric cylinder. In this case, all the above-mentioned points of intersection of the dispersion curves with the Cherenkov resonance line correspond to the excitation of the bulk-surface waves only.

Since the nanotube significantly affects only the modes with $n = 1$ and $s = 1$, it is interesting to carry out numerical estimates of the electron energy loss for the case of excitation of the HE_{11} and EH_{11} bulk-surface waves. As an example, we present the magnetic field dependence of the partial dimensionless losses $\overline{W} = -(dW/dt)/(dW/dt)_0$ due to the excitation of the EH_{11} wave (see the red solid curve 1 in Fig. 6), where $(dW/dt)_0 = e^2c/\rho_c^2 \approx 2.8 \times 10^{-5}$ W. One can see that the electron energy loss oscillates with a change in the number η of magnetic flux quanta through the nanotube cross section with a period equal to one magnetic flux quantum. The extrema points in the dependence $\overline{W}(\eta)$ correspond to the turning points on the dispersion curves $\Omega(Q)$ built for corresponding values of η. As is also evident from Fig. 6, the values of η at the extrema points in the dependence $\overline{W}(\eta)$ are the same as the values of η at which the jumps in the magnetic field dependence of the number k of filled electron energy subzones occur (see the blue dashed curve 2 in Fig. 6).

B. Increment

For numerical analysis of the dependence of the increment of kinetic instability on the number of magnetic flux quanta, we choose the following parameters of the tubular beam: $n_0^B = 10^{16}$ m^{-3}, $T = 2.2 \times 10^4$ K, which corresponds to the average thermal velocity of the beam electrons ($v_T \approx 10^6$ m/s and $v_0/c \approx 0.33$). In this case, the beam is nonrelativistic because the condition $1 - \sqrt{1 - v_0^2/c^2} \approx 0.06 \ll 1$ holds.

The dependence of relative increment γ/Ω of the kinetic instability due to the excitation of EH_{11} bulk-surface waves on the number η of magnetic flux quanta (solid red curve 1) and the dependence $\Omega(\eta)$ (dashed blue curve 2) are shown in Fig. 7 for $Q = 1.79 \times 10^{-3}$, $\rho_e = 1.1\rho_c$, $\nu = 3 \times 10^{11}$ s^{-1}. As seen from this figure, the dependence γ/Ω on η has the form of a periodic set of narrow maxima with a period equal to one magnetic flux quantum. The positions of these maxima coincide with the positions of the maxima in the dependence $\Omega(\eta)$. This means that an external dc magnetic field can significantly influence the interaction efficiency of the beam of charged particles with the electron plasma in the nanotube. This, in turn, makes it possible to propose the studied structure for the creation of nanoscale oscillators and amplifiers effectively controlled by a dc magnetic field. Recall that the generation of electromagnetic waves is possible in the case when the beam excites the electromagnetic waves with negative dispersion. It is remarkable that the Aharonov-Bohm effect can significantly affect the macroscopic phenomenon of the beam instability.

V. CONCLUSIONS

The problem of electron and tubular electron beam interaction with electromagnetic waves in a semiconductor nanotube with a dielectric filling placed in a coaxial dc magnetic field has been theoretically examined. In this study, the electron collisions in the nanotube should be taken into account, and first we analyzed the transformation of the eigenmodes spectrum due to these collisions. The main transformation consists in the emergence of dissipative (leaky) waves (similar to Zenneck-Sommerfeld's waves in the plane geometry) with phase velocities greater than the speed of light in the vacuum and in the disappearance of frequency gaps in the spectrum. However, in doing so the sections in the dispersion curves with negative dispersion, existing in the collisionless regime, are kept. We have found that the number of such sections with negative slope oscillates with a change in the number of the magnetic flux quanta through the nanotube with a period equal to one magnetic flux quantum. The presence of characteristic bends on the dependence of the nanotube conductivity on the longitudinal wave number are shown to be responsible for the appearance of the turning points on the dispersion curves for the eigenmodes.

The analysis of the interaction of a moving nonrelativistic electron with both the bulk-surface and surface electromagnetic waves was carried out. We have shown that the electron energy loss due to the wave excitation oscillates when changing the magnetic flux through the nanotube with a period equal to one magnetic flux quantum, which is a manifestation of the Aharonov-Bohm effect.

Using the so-called energy approach, we obtained the analytical expression for the increment of the kinetic instability due to the wave interaction with a tubular electron beam. The numerical analysis of the dependence of this increment on the number of magnetic flux quanta through the nanotube shows the presence of oscillations, which have the form of a set of narrow periodically located maxima, with a period equal to one magnetic flux quantum. This means that, first, the Aharonov-Bohm effect clearly manifests in the macroscopic phenomenon of beam instability, and second, it is possibile to use this phenomenon to create nanoscale amplifiers and oscillators of terahertz radiation controlled by an external dc magnetic field.

ACKNOWLEDGMENTS

We thank Dr. G. I. Rashba for useful discussions. This work was supported by the National Research Foundation of Ukraine through Project No. 2020.02/0149, "Quantum phenomena in the interaction of electromagnetic waves with solid-state nanostructures."

[1] Y. Aharonov and D. Bohm, Phys. Rev. **115**, 485 (1959).
[2] R. G. Chambers, H. H. Wills, Phys. Rev. Lett. **5**, 3 (1960).
[3] G. Möllenstedt and W. Bayh, Naturwissenschaften **49**, 81 (1962).
[4] A. Tonomura, N. Osakabe, T. Matsuda, T. Kawasaki, J. Endo, S. Yano, and H. Yamada, Phys. Rev. Lett. **56**, 792 (1986).
[5] H. Batelaan and A. Tonomura, Phys. Today **62**(9), 38 (2009).
[6] R. A. Webb, S. Washburn, C. P. Umbach, and R. B. Laibowitz, Phys. Rev. Lett. **54**, 2696 (1985).
[7] J. Dauber, M. Oellers, F. Venn, A. Epping, K. Watanabe, T. Taniguchi, F. Hassler, and C. Stampfer, Phys. Rev. B **96**, 205407 (2017).
[8] L. L. Li, D. Moldovan, P. Vasilopoulos, and F. M. Peeters, Phys. Rev. B **95**, 205426 (2017).
[9] B. Rzeszotarski, A. Mreńca-Kolasińska, and B. Szafran, Phys. Rev. B **101**, 115308 (2020).
[10] O. V. Kibis, H. Sigurdsson, and I. A. Shelykh, Phys. Rev. B **91**, 235308 (2015).
[11] R. Kozlovsky, A. Graf, D. Kochan, K. Richter, and C. Gorini, Phys. Rev. Lett. **124**, 126804 (2020).
[12] K. Luo, H. Geng, L. Sheng, W. Chen, and D. Y. Xing, Phys. Rev. B **104**, 085427 (2021).
[13] T. Haug, H. Heimonen, R. Dumke, L.-C. Kwek, and L. Amico, Phys. Rev. A **100**, 041601(R) (2019).
[14] H. Li and W. Yi, Phys. Rev. A **106**, 053311 (2022).
[15] M. M. Shulaker, G. Hills, N. Patil, H. Wei, H.-Y. Chen, H.-S. P. Wong, and S. Mitra, Nature (London) **501**, 526 (2013).
[16] R. M. Wilson, Phys. Today **70**(9), 14 (2017).
[17] A. Bachtold, C. Strunk, J.-P. Salvetat, J.-M. Bonard, L. Forroó, T. Nussbaumer, and C. Schoénenberger, Nature (London) **397**, 673 (1999).
[18] J. Kim, J.-R. Kim, J.-O. Lee, J. W. Park, H. M. So, N. Kim, K. Kang, K.-H. Yoo, and J.-J. Kim, Phys. Rev. Lett. **90**, 166403 (2003).
[19] S. Uryu and T. Ando, Phys. Rev. B **77**, 205407 (2008).
[20] S.-B. Chiu, A. Mreńca-Kolasińska, K. L. Lei, C.-H. Chiu, W.-H. Kang, S.-C. Chen, and M.-H. Liu, Phys. Rev. B **105**, 195416 (2022).
[21] Y. Dahman, *Nanotechnology and Functional Materials for Engineers* (Elsevier, Toronto, 2017).
[22] *Emerging Nanotechnologies in Rechargeable Energy Storage Systems*, edited by L. M. Rodriguez-Martinez and N. Omar (Elsevier, Amsterdam, 2017).
[23] *Nanosilicon*, edited by V. Kumar (Elsevier Science, 2008).
[24] J. Sha, J. J. Niu, X. Y. Ma, J. Xu, X. B. Zhang, Q. Yang, and D. Yang, Adv. Mater. **14**, 1219 (2002).
[25] S. Y. Jeong, J. Y. Kim, H. D. Yang, B. N. Yoon, S. H. Choi, H. K. Kang, C. W. Yang, and Y. H. Lee, Adv. Mater. **15**, 1172 (2003).
[26] G. G. Guzman-Verri and L. C. Lew Yan Voon, Phys. Rev. B **76**, 075131 (2007).
[27] X. Huang, R. Gonzalez-Rodriguez, R. Rich, Z. Gryczynski, and J. L. Coffer, Chem. Commun. **49**, 5760 (2013).
[28] A. I. Vedernikov, A. O. Govorov, and A. V. Chaplik, J. Exp. Theor. Phys. **93**, 853 (2001).
[29] Yu. O. Averkov, Yu. V. Prokopenko, and V. M. Yakovenko, Low Temp. Phys. **48**, 32 (2022).
[30] Yu. O. Averkov, Yu. V. Prokopenko, V. M. Yakovenko, and V. A. Yampol'skii, Low Temp. Phys. **49**, 3 (2023).
[31] J. Zenneck, Ann. Phys. **328**, 846 (1907).
[32] *Handbook of Mathematical Functions with Formulas, Graphs, and Mathematical Tables*, edited by M. Abramowitz and I. Stegun (National Bureau of Standards, Washington, DC, 1964).
[33] A. M. Ermolaev, S. V. Kofanov, and G. I. Rashba, Adv. Condens. Matter Phys. **2011**, 901848 (2011).
[34] Yu. V. Prokopenko and Yu. F. Filipov, Tech. Phys. **47**, 731 (2002).
[35] L. D. Landau and E. M. Lifshitz, *Electrodynamics of Continuous Media* (Pergamon, Oxford, 1984).
[36] E. Snitzer, J. Opt. Soc. Am. **51**, 491 (1961).
[37] A. Sommerfeld, Ann. Phys. Chem. **303**, 233 (1899).
[38] G. Goubau, J. Appl. Phys. **21**, 1119 (1950).
[39] B. G. Martin and R. F. Wallis, Phys. Rev. B **13**, 3339 (1976).
[40] T.-I. Jeon and D. Grischkowsky, Appl. Phys. Lett. **88**, 061113 (2006).
[41] L. Chusseau and J.-P. Guillet, J. Infr. Milli. Terahz. Waves **33**, 174 (2012).
[42] S. K. Oruganti, F. Liu, D. Paul, J. Liu, J. Malik, K. Feng, H. Kim, Y. Liang, T. Thundat, and F. Bien, Sci. Rep. **10**, 925 (2020).
[43] J. D. Jackson, *Classical Electrodynamics*, 3rd ed. (Wiley, Berkeley, 1999).
[44] R. B. Miller, *An Introduction to the Physics of Intense Charged Particle Beams* (Plenum, New York, 1982).
[45] V. M. Yakovenko, M. V. Burtyka, and I. V. Yakovenko, Int. J. Infr. Milli. Waves **17**, 559 (1996).